Hyperspectral Unmixing Using Double Reweighted Sparse Regression and Total Variation

Rui Wang, Heng-Chao Li, *Senior Member, IEEE*, Aleksandra Pizurica, *Member, IEEE*, Jun Li, *Senior Member, IEEE*, Antonio Plaza, *Fellow, IEEE*, and William J. Emery, *Fellow, IEEE*

***Abstract*— Spectral unmixing is an important technique in hyperspectral image applications. Recently, sparse regression has been widely used in hyperspectral unmixing, but its performance is limited by the high mutual coherence of spectral libraries. To address this issue, a new sparse unmixing algorithm, called double reweighted sparse unmixing and total variation (TV), is proposed in this letter. Specifically, the proposed algorithm enhances the sparsity of fractional abundances in both spectral and spatial domains through the use of double weights, where one is used to enhance the sparsity of endmembers in spectral library, and the other is introduced to improve the sparsity of fractional abundances. Moreover, a TV-based regularization is further adopted to explore the spatial–contextual information. As such, the simultaneous utilization of both double reweighted l_1 minimization and TV regularizer can significantly improve the sparse unmixing performance. Experimental results on both synthetic and real hyperspectral data sets demonstrate the effectiveness of the proposed algorithm both visually and quantitatively.**

***Index Terms*— Double weights, hyperspectral unmixing, sparse regression, total variation (TV).**

I. Introduction

DUE to low spatial resolution as well as the presence of microscopic material mixing and multiple scattering, mixed pixels are commonly present in hyperspectral imagery. To some extent, the existence of mixed pixels restricts the processing and application of hyperspectral images in practice [1], [2]. Thus, spectral unmixing has been an important technique for hyperspectral data exploitation, which decomposes a mixed pixel into a collection of constituent materials called endmembers and their corresponding abundances [3]. To date, many methods have been proposed for hyperspectral unmixing, most of which are based on the linear mixing model (LMM). It assumes that the observed pixel spectrum is a linear combination of endmember signatures weighted by their associated fractional abundances. From LMM, geometrical and statistical methods are the two most widely used classes of techniques [5]. However, they generally require the estimation of the number of endmembers and/or the presence of pure pixels in a given scene. Recently, sparse unmixing [6] has been proposed to overcome these issues, which opens up new perspective to perform spectral unmixing. As a semisupervised approach, it amounts to finding the optimal subset of signatures from a (potentially very large) spectral library that can best model each mixed pixel. The sparse unmixing algorithm via variable splitting and augmented Lagrangian (SUnSAL) [6], [7] is the seminal work developed for this purpose, making use of the fact that there are typically only a few endmembers inside a pixel compared with the large spectral library. Nevertheless, the high correlation of spectral libraries imposes some limitations to the performance of SUnSAL. To mitigate them, Iordache *et al.* [8] introduce the total variation (TV) regularizer to integrate the spatial–contextual information of hyperspectral data and propose the SUnSAL-TV algorithm from SUnSAL. However, SUnSAL-TV may yield oversmoothness and blurred boundaries. From different perspectives, the joint sparsity is also investigated to develop collaborative SUnSAL (CLSUnSAL) in [9] by assuming that all the observed pixels in a hyperspectral image have the same active set of endmembers. In [10] and [11], an l_p $(0 < p < 1)$ norm is utilized to replace the standard l_1 norm in SUnSAL for the purpose of yielding sparser solution. Though showing some unmixing performance improvement, this sparsity-promoting norm strategy only exploits the column sparsity of the abundance matrix.

Inspired by the success of the reweighted l_1 minimization for enhancing sparsity [12], a new sparse unmixing algorithm, called double reweighted sparse unmixing and TV (DRSU-TV), is proposed in this letter. The proposed DRSU-TV simultaneously explores the spectral–spatial dual sparsity as well as the spatial smoothness of fractional abundances. The main contributions of this letter can be summarized as follows.

1) A double reweighted sparse unmixing model is formulated. Specifically, one weight is introduced to enhance the column sparsity of the fractional abundances in the sense that a hyperspectral image typically contains fewer endmembers compared with the overcomplete spectral dictionary, whereas the other weight is to promote sparsity along the abundance vector corresponding to each endmember.

Manuscript received December 3, 2016; revised March 24, 2017; accepted April 24, 2017. This work was supported by the National Natural Science Foundation of China under Grant 61371165. *(Corresponding author: Heng-Chao Li.)*

R. Wang and H.-C. Li are with the Sichuan Provincial Key Laboratory of Information Coding and Transmission, Southwest Jiaotong University, Chengdu 610031, China (e-mail: lihengchao_78@163.com).

A. Pizurica is with the Department of Telecommunications and Information Processing, Ghent University, 9000 Ghent, Belgium.

J. Li is with the Guangdong Provincial Key Laboratory of Urbanization and Geo-Simulation, Sun Yat-sen University, Guangzhou 510275, China.

A. Plaza is with the Hyperspectral Computing Laboratory, Department of Technology of Computers and Communications, Escuela Politécnica, University of Extremadura, 10071 Cáceres, Spain.

W. J. Emery is with the Department of Aerospace Engineering Sciences, University of Colorado, Boulder, CO 80309 USA.

Color versions of one or more of the figures in this letter are available online at http://ieeexplore.ieee.org.

Digital Object Identifier 10.1109/LGRS.2017.2700542

2) In view of the importance of considering the spatial information for sparse unmixing, a TV-based regularization is further incorporated for encouraging spatial homogeneity while preserving discontinuities. Thus, the spatial information is also investigated. The simultaneous utilization of both TV regularizer and double reweighted l_1 minimization can significantly improve the sparse unmixing performance.

II. Methodology

This section details the proposed DRSU-TV algorithm, including the model formulation and its optimization by the alternating direction method of multipliers (ADMM) [13].

A. Formulation of Proposed DRSU-TV Model

Let $\mathbf{A} \in \mathbb{R}^{L\times m}$ denote a spectral library having m spectral signatures. Instead of the spectral endmembers directly extracted or generated from the hyperspectral data, linear sparse unmixing amounts to finding the optimal subset of spectral samples in $\mathbf{A}$ to best model each mixed pixel in the scene. Typically, we have

$$\mathbf{y} = \mathbf{A}\mathbf{x} + \mathbf{n} \tag{1}$$

where $\mathbf{y}$ and $\mathbf{n}$ are the observed spectral and noise vectors, respectively. $\mathbf{x} \in \mathbb{R}^{m\times 1}$ denotes the fractional abundance vector with regard to the library $\mathbf{A}$, subject to two physical constraints: abundance nonnegativity constraint and abundance sum-to-one constraint (ASC) (i.e., $\mathbf{x} \geq 0$ and $\sum_{i=1}^{m} x_i = 1$). Here, only a few of the signatures contained in $\mathbf{A}$ are likely contributing to the observed mixed pixel, such that $\mathbf{x}$ contains many zero values (i.e., it is *sparse*).

In [6] and [7], sparse unmixing is formulated as an $l_2 - l_1$ norm optimization problem by surrogating the l_0 norm of the original regularization, that is

$$\min_{\mathbf{x}} \frac{1}{2}\|\mathbf{y} - \mathbf{A}\mathbf{x}\|_2^2 + \lambda\|\mathbf{x}\|_1, \quad \text{s.t. } \mathbf{x} \geq 0 \tag{2}$$

with λ being a regularization parameter. The first term accounts for the pixel reconstruction error, while the second term imposes sparsity in the solution. The ASC constraint is not explicitly added in (2) because of the following: 1) it should be replaced by a generalized ASC due to strong signature variability in a real image, which will be automatically imposed by the nonnegativity of the sources (i.e., $\mathbf{x} \geq 0$) [7] and 2) the combination of ASC with the l_1-norm regularization does not induce sparsity [11]. The SUnSAL algorithm is proposed to solve (2) in [6] and [7], which, however, is heavily influenced by the high correlation of spectral libraries due to the underdetermined nature of (2). To admit a sufficiently sparse solution for sparse unmixing will guarantee a more accurate abundance estimation. In this context, given the spectral library, the sparsity-promoting norm regularization seems to be a natural way. In [9], CLSUnSAL imposes the joint sparsity with an $l_{2,1}$ mixed norm among the endmembers simultaneously for all of the pixels. In [10] and [11], the l_p $(0 < p < 1)$ norm is proposed as an alternative to the l_1 norm in SUnSAL for the purpose of promoting sparsity besides allowing the ASC. Nevertheless, this kind of strategy only exploit the sparsity of actual spectral signatures in spectral library, i.e., that among columns of the abundance matrix.

From a different perspective, we propose to utilize the reweighted l_1-norm idea originally introduced in [12], which can efficiently enhance the sparsity of the solution and improve the estimation performance over the l_1 norm. This way we investigate the spectral–spatial dual sparsity to construct a double reweighted sparse unmixing model. For any given hyperspectral image with n pixels, (1) can be written in a compact matrix form, i.e., $\mathbf{Y} = \mathbf{A}\mathbf{X} + \mathbf{N}$, where $\mathbf{Y} = [\mathbf{y}_1, \cdots, \mathbf{y}_n] \in \mathbb{R}^{L\times n}$ is the observed data matrix, and $\mathbf{X} = [\mathbf{x}_1, \cdots, \mathbf{x}_n] \in \mathbb{R}^{m\times n}$ and $\mathbf{N} = [\mathbf{n}_1, \cdots, \mathbf{n}_n] \in \mathbb{R}^{L\times n}$, respectively, refer to the abundance and noise matrices. The sparse unmixing of double reweighted l_1-norm minimization is formulated as follows:

$$\min_{\mathbf{X}} \frac{1}{2}\|\mathbf{Y} - \mathbf{A}\mathbf{X}\|_F^2 + \lambda\|\mathbf{W_2} \odot (\mathbf{W_1}\mathbf{X})\|_{1,1}, \quad \text{s.t. } \mathbf{X} \geq 0 \tag{3}$$

where the operator $\odot$ denotes the elementwise multiplication (i.e., Hadamard product) of two variables, and $\|\mathbf{X}\|_{1,1} \equiv \sum_{j=1}^{n} \|\mathbf{x}_j\|_1$ with $\mathbf{x}_j$ being the jth column of $\mathbf{X}$.

In (3), the first weight $\mathbf{W_1}$ is introduced to promote the column sparsity of the fractional abundances in the sense that a hyperspectral image typically contains fewer endmembers compared with the overcomplete spectral dictionary. Due to the unavailability of $\mathbf{X}$, we adopt an iterative reweighted approach [12] to design $\mathbf{W_1}$

$$\mathbf{W}_1^{(t+1)} = \operatorname{diag}\left[\frac{1}{\|\mathbf{X}^{(t)}(1,:)\|_1 + \epsilon}, \cdots, \frac{1}{\|\mathbf{X}^{(t)}(m,:)\|_1 + \epsilon}\right] \tag{4}$$

in which $\epsilon > 0$ is a stabilization parameter and $\mathbf{X}^{(t)}(i,:)$ represents the ith row of $\mathbf{X}$ estimated in the tth iteration. Here, $\mathbf{W_1} \in \mathbb{R}^{m\times m}$ exhibits a diagonal form, with each entry being inversely proportional to the l_1-norm value of the corresponding abundance vector estimated from the previous iteration. This suggests that large weights could be used to discourage nonzero row vectors in the recovered abundance matrix, whereas small weights could be used to encourage nonzero row vectors. Although $\mathbf{W_1}$ enhances the sparsity of endmember spectra in library $\mathbf{A}$, it equally treats all of the entries in each abundance vector. Actually, the hyperspectral abundance maps are inherently sparse. That is to say, it is generally unlikely that the same material is present in every pixel of the given scene. Therefore, the second weight $\mathbf{W_2}$ is proposed to promote sparsity along the abundance vector corresponding to each endmember. Similarly, we define its element of $\mathbf{W_2} \in \mathbb{R}^{m\times n}$ as follows:

$$\mathbf{W}_2^{(t+1)}(i,j) = \frac{1}{\mathbf{X}^{(t)}(i,j) + \epsilon}. \tag{5}$$

Obviously, the large weights of $\mathbf{W}_2$ discourage nonzero entries in the estimated abundance, and vice versa. As such, the double reweighted l_1 norm will simultaneously give rise to the sparsity promotion of nonzero abundance vectors as well as that of their nonzero entries by iteratively penalizing the components with the low row-norm and/or low abudance value.

Furthermore, in view of the importance of considering the spatial information for sparse unmixing [8], we consider the

fact that hyperspectral images often exhibit high-spatial correlation among the neighboring pixels, implying that the abundance maps can be regarded as piecewise smooth. A TV-based regularization is further incorporated in (3) for encouraging spatial homogeneity while preserving discontinuities. As such, we have the following DRSU-TV model, that is

$$\min_{\mathbf{X}} \frac{1}{2}\|\mathbf{Y}-\mathbf{AX}\|_F^2 + \lambda\|\mathbf{W_2}\odot(\mathbf{W_1X})\|_{1,1} + \lambda_{\mathrm{TV}}\mathrm{TV}(\mathbf{X}), \quad \text{s.t. } \mathbf{X}\geq 0 \tag{6}$$

where $\mathrm{TV}(\mathbf{X}) \equiv \sum_{j,k\in\varepsilon}\|\mathbf{x}_j-\mathbf{x}_k\|$ [8]. It is worth noting that $\mathbf{W_1}$ and $\mathbf{W_2}$ make DRSU-TV different from existing algorithms. But when $\mathbf{W_1}$ and $\mathbf{W_2}$ are set to the identity matrix and the all-ones matrix, respectively, the proposed DRSU-TV algorithm will reduce to SUnSAL-TV as well as SUnSAL further with $\lambda_{\mathrm{TV}}=0$.

B. Optimization by the ADMM

To solve (6), it is proposed to adopt the ADMM [13]. Specifically, following [7]–[9] and [13], we have the constrained equivalent formulation of (6), given by

$$\begin{aligned}\min_{\mathbf{X},\mathbf{V_1},\mathbf{V_2},\mathbf{V_3},\mathbf{V_4},\mathbf{V_5}} & \frac{1}{2}\|\mathbf{Y}-\mathbf{V_1}\|_F^2 + \lambda\|\mathbf{W}_2\odot\mathbf{V_2}\|_{1,1} \\ & + \lambda_{\mathrm{TV}}\|\mathbf{V_4}\|_{1,1} + \imath_{R_+}(\mathbf{V_5}) \\ \text{s.t. } & \mathbf{V}_1=\mathbf{AX},\ \mathbf{V}_2=\mathbf{W_1X},\ \mathbf{V}_3=\mathbf{X},\ \mathbf{V}_4=\mathbf{HV_3},\ \mathbf{V}_5=\mathbf{X}\end{aligned} \tag{7}$$

where $\mathbf{H}$ includes two linear operators computing the horizontal and vertical differences, respectively [8], and $\imath_{R_+}(\mathbf{X}) = \sum_{j=1}^{n}\imath_{R_+}(\mathbf{x}_j)$ is the indicator function with $\imath_{R_+}(\mathbf{x}_j)=0$ when $\mathbf{x}_j$ belongs to the nonnegative orthant, otherwise $\imath_{R_+}(\mathbf{x}_j)=+\infty$. Then, (7) can be further expressed in a compact form

$$\min_{\mathbf{X},\mathbf{V}} g(\mathbf{V}) \text{ s.t. } \mathbf{GX}+\mathbf{BV}=0 \tag{8}$$

where $\mathbf{V}=(\mathbf{V_1},\mathbf{V_2},\mathbf{V_3},\mathbf{V_4},\mathbf{V_5})$, $g(\mathbf{V}) = (1/2)\|\mathbf{Y}-\mathbf{V_1}\|_F^2 + \lambda\|\mathbf{W}_2\odot\mathbf{V_2}\|_{1,1} + \lambda_{\mathrm{TV}}\|\mathbf{V_4}\|_{1,1} + \imath_{R_+}(\mathbf{V_5})$, and $\mathbf{G}$ and $\mathbf{B}$ are, respectively, given by

$$\mathbf{G}=\begin{bmatrix}\mathbf{A}\\ \mathbf{W}_1\\ \mathbf{I}\\ \mathbf{0}\\ \mathbf{I}\end{bmatrix},\quad \mathbf{B}=\begin{bmatrix}-\mathbf{I} & 0 & 0 & 0 & 0\\ 0 & -\mathbf{I} & 0 & 0 & 0\\ 0 & 0 & -\mathbf{I} & 0 & 0\\ 0 & 0 & \mathbf{H} & -\mathbf{I} & 0\\ 0 & 0 & 0 & 0 & -\mathbf{I}\end{bmatrix}. \tag{9}$$

By introducing the scaled Lagrange multipliers $\mathbf{D}=(\mathbf{D_1},\mathbf{D_2},\mathbf{D_3},\mathbf{D_4},\mathbf{D_5})$, the augmented Lagrangian associated with the optimization of (8) is written as

$$\mathcal{L}(\mathbf{X},\mathbf{V},\mathbf{D}) \equiv g(\mathbf{V}) + \frac{\mu}{2}\|\mathbf{GX}+\mathbf{BV}-\mathbf{D}\|_F^2 \tag{10}$$

where $\mu>0$ is a penalty parameter. The ADMM iteratively minimizes $\mathcal{L}(\mathbf{X},\mathbf{V},\mathbf{D})$ with respect to $\mathbf{X}$ and $\mathbf{V}$ followed by an update of $\mathbf{D}$ in three consecutive steps. Thus, we have

$$\begin{aligned}\mathbf{X}^{(t+1)} = & \left(\mathbf{A}^T\mathbf{A}+\left(\mathbf{W}_1^{(t)}\right)^T\mathbf{W}_1^{(t)}+2\mathbf{I}\right)^{-1} \\ & \times\left(\mathbf{A}^T\left(\mathbf{V}_1^{(t)}+\mathbf{D}_1^{(t)}\right)+\left(\mathbf{W}_1^{(t)}\right)^T\left(\mathbf{V}_2^{(t)}+\mathbf{D}_2^{(t)}\right)\right. \\ & \left.+\left(\mathbf{V}_3^{(t)}+\mathbf{D}_3^{(t)}\right)+\left(\mathbf{V}_5^{(t)}+\mathbf{D}_5^{(t)}\right)\right)\end{aligned} \tag{11}$$

and then the optimization for $\mathbf{V}$ is performed as

$$\begin{cases}\mathbf{V}_1^{(t+1)} = \dfrac{1}{1+\mu}\left[\mathbf{Y}+\mu\left(\mathbf{AX}^{(t+1)}-\mathbf{D}_1^{(t)}\right)\right] \\ \mathbf{V}_2^{(t+1)} = \mathrm{soft}_{\lambda/\mu\mathbf{W}_2^{(t)}}\left(\mathbf{W}_1^{(t)}\mathbf{X}^{(t+1)}-\mathbf{D}_2^{(t)}\right) \\ \mathbf{V}_3^{(t+1)} = \mathbf{M}\left(\mathbf{X}^{(t+1)}-\mathbf{D}_3^{(t)}+\mathbf{H}^T\left(\mathbf{V}_4^{(t)}+\mathbf{D}_4^{(t)}\right)\right) \\ \mathbf{V}_4^{(t+1)} = \mathrm{soft}_{\lambda_{\mathrm{TV}}/\mu}\left(\mathbf{HV}_3^{(t+1)}-\mathbf{D}_4^{(t)}\right) \\ \mathbf{V}_5^{(t+1)} = \max\left(\mathbf{X}^{(t+1)}-\mathbf{D}_5^{(t)},0\right)\end{cases} \tag{12}$$

where $\mathrm{soft}_{\lambda/\mu\mathbf{W}_2^{(t)}}(\cdot)$ and $\mathrm{soft}_{\lambda_{\mathrm{TV}}/\mu}(\cdot)$, respectively, denote the nonuniform and uniform soft thresholding operators [14], [15], and $\mathbf{M}=(\mathbf{H}^T\mathbf{H}+\mathbf{I})^{-1}$. Finally, the scaled Lagrange multipliers in $\mathbf{D}$ are sequentially updated as follows:

$$\begin{cases}\mathbf{D}_1^{(t+1)} = \mathbf{D}_1^{(t)}-\mathbf{AX}^{(t+1)}+\mathbf{V}_1^{(t+1)} \\ \mathbf{D}_2^{(t+1)} = \mathbf{D}_2^{(t)}-\mathbf{W}_1^{(t)}\mathbf{X}^{(t+1)}+\mathbf{V}_2^{(t+1)} \\ \mathbf{D}_3^{(t+1)} = \mathbf{D}_3^{(t)}-\mathbf{X}^{(t+1)}+\mathbf{V}_3^{(t+1)} \\ \mathbf{D}_4^{(t+1)} = \mathbf{D}_4^{(t)}-\mathbf{HV_3}^{(t+1)}+\mathbf{V}_4^{(t+1)} \\ \mathbf{D}_5^{(t+1)} = \mathbf{D}_5^{(t)}-\mathbf{X}^{(t+1)}+\mathbf{V}_5^{(t+1)}.\end{cases} \tag{13}$$

III. Experimental Results and Discussion

In this section, unmixing experiments are performed on both the synthetic and real hyperspectral images to illustrate the effectiveness of our proposed DRSU-TV algorithm. Results of SUnSAL, CLSUnSAL, and SUnSAL-TV are given for comparative purposes. To make a fair comparison, the quasi-optimal parameter setting for the underlying regularization parameters (i.e., λ or/and λ_{TV}) of each algorithm is found in a finite set {0.0005, 0.005, 0.05, 0.1, 0.2, 0.3, 0.4, 0.5, 1.0, 1.5, 2}. For DRSU-TV, $\mathbf{W}_1$ and $\mathbf{W}_2$ are, respectively, initialized to be the identity matrix and the all-ones matrix.

A. Synthetic Data Experiments

The spectral library used in these synthetic image experiments is $\mathbf{A}\in\mathbb{R}^{224\times 240}$, which is generated by randomly selecting 240 different materials from the U.S. Geological Survey (USGS) library. The USGS library is available online at http://speclab.cr.usgs.gov/spectral.lib06. It comprises spectral signatures with reflectance values given in 224 spectral bands and distributed uniformly over the interval 0.4–2.5 μm. Two different simulated data cubes are generated with this spectral library.

1) *Simulated Data Cube 1 (DC1):* The first simulated data have 75×75 pixels and 224 bands per pixel based on LMM by using five randomly chosen spectral signatures from the library $\mathbf{A}$ as the endmembers and generating the abundances following the methodology of [8].
2) *Simulated Data Cube 2 (DC2):* These simulated data contain 70×70 pixels and 224 bands per pixel. Nine spectral signatures are randomly selected from the library $\mathbf{A}$ as the endmembers and generating the abundances according to the Gaussian fields method [16].

Finally, DC1 and DC2 are degraded by Gaussian noise with three levels of the signal-to-noise ratio, i.e., 20, 30, and 40 dB.

TABLE I
SRE (IN DECIBELS) VALUES ON THE SYNTHETIC DATA SETS

DC1	SUnSAL	CLSUnSAL	SUnSAL-TV	DRSU-TV
20dB	3.4982	4.7750	10.8890	21.8182
30dB	7.6253	12.2891	18.7212	29.1222
40dB	15.7232	21.5225	28.1640	40.7857
DC2	SUnSAL	CLSUnSAL	SUnSAL-TV	DRSU-TV
20dB	5.3238	5.7104	8.0866	12.9224
30dB	11.0013	11.9338	16.4257	27.1372
40dB	16.7371	17.9520	19.9911	33.0430

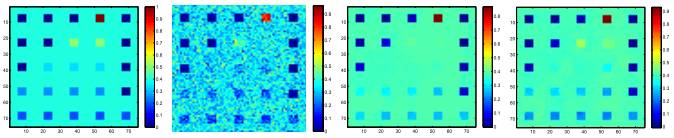

(a) (b) (c) (d)

Fig. 1. Abundance maps obtained by different unmixing methods for the fifth endmember in DC1 with SNR = 20 dB. (a) Ground truth. (b) CLSUnSAL. (c) SUnSAL-TV. (d) DRSU-TV.

For quantitative evaluation, the signal-to-reconstruction error (SRE) is adopted as the objective metric [7]. The SRE in decibels is defined as $\text{SRE} = 10\log_{10}(E[\|\mathbf{x}\|_2^2]/E[\|\mathbf{x}-\hat{\mathbf{x}}\|_2^2])$, where $\hat{\mathbf{x}}$ is the estimation of the true fractional abundance vector $\mathbf{x}$ and $E[\cdot]$ stands for expectation function. This metric indicates the quality of the reconstruction of spectral mixtures, for which the larger its value is, the better the performance of the algorithm for recovering the abundances is.

Table I shows the SRE (dB) results obtained by four sparse unmixing algorithms on DC1 and DC2 under all considered SNR levels. From Table I, we can observe that the overall performance of each unmixing algorithm tends to degrade as the noise level increases. SUnSAL yields the worst unmixing performance, followed by CLSUnSAL. Comparatively speaking, SUnSAL-TV and DRSU-TV perform better by incorporating the spatial–contextual information of the hyperspectral data. Moreover, DRSU-TV is obviously superior to SUnSAL-TV no matter what the level of noise is for two synthetic data sets. This is as expected, since $\mathbf{W}_1$ improves the ability of identifying endmembers, while both $\mathbf{W}_2$ and TV regularizer can further guarantee the quality of the abundance images. Nevertheless, we would like to note that the SRE gain of DRSU-TV over SUnSAL-TV is dependent on the noise level and the number of endmembers. For the case of DC2 with SNR = 20 dB, the unmixing is becoming difficult, such that the resulting gain decreases to about 5 dB.

Meanwhile, we take SNR = 20 dB as an example for the purpose of visual interpretation. However, limited to the space and in view of the relatively worse results of SUnSAL, Figs. 1 and 2 show the abundance maps estimated by the CLSUnSAL, SUnSAL-TV, and DRSU-TV algorithms, respectively, for the fifth endmember in DC1 and for the first, second, and fifth endmembers in DC2. In addition, the corresponding fractional abundance estimations obtained for each endmember material in $\mathbf{A}$ (as a function of pixel index in scenes DC1 and DC2 with SNR = 20 dB), along with the ground-truth abundances, are shown in Figs. 3 and 4, in which the

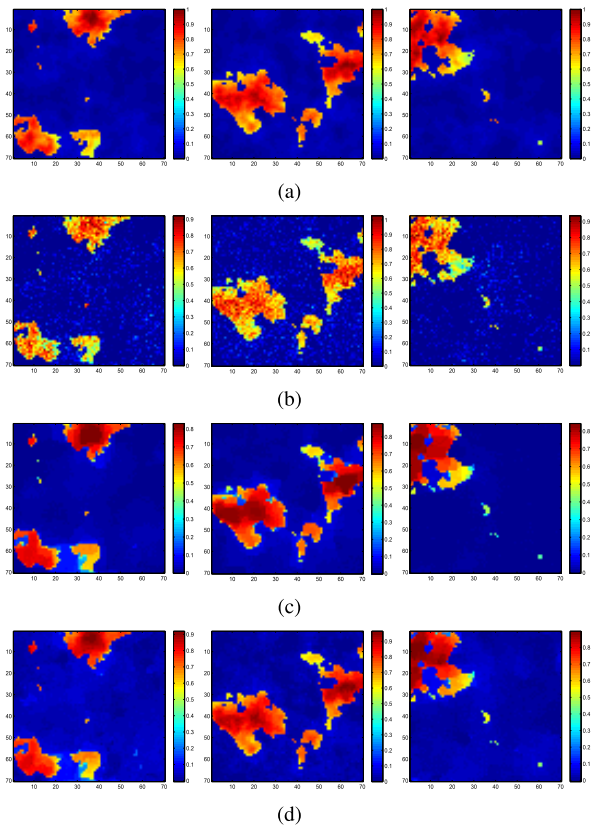

(a) (b) (c) (d)

Fig. 2. Abundance maps obtained by different unmixing methods for the first, second, and fifth endmembers in DC2 with SNR = 20 dB. (a) Ground truth. (b) CLSUnSAL. (c) SUnSAL-TV. (d) DRSU-TV.

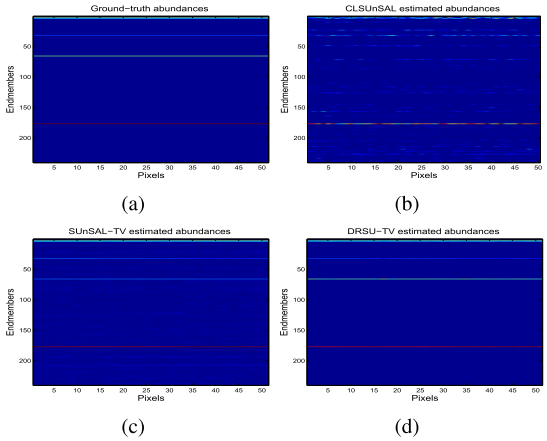

(a) (b) (c) (d)

Fig. 3. Ground-truth and estimated abundances obtained for each endmember material in the spectral library for 50 pixels in DC1 when SNR = 20 dB.

line denotes the abundance of a certain endmember in only 50 selected pixels. From Figs. 1 and 2, it can be observed that the abundance images obtained by CLSUnSAL seem to be noisy, although the row sparsity constraint promotes the solutions of CLSUnSAL. On the contrary, the estimated abundances of SUnSAL-TV and DRSU-TV are more accurate and have a better visual effect. However, a close look of Figs. 1(c) and (d) and 2(c) and (d) reveals that DRSU-TV presents less blurring and oversmoothness in the abundance estimations than SUnSAL-TV, whose abundance values have better consistency with the ground-truth values because of considering the spatial information and enhancing the sparsity

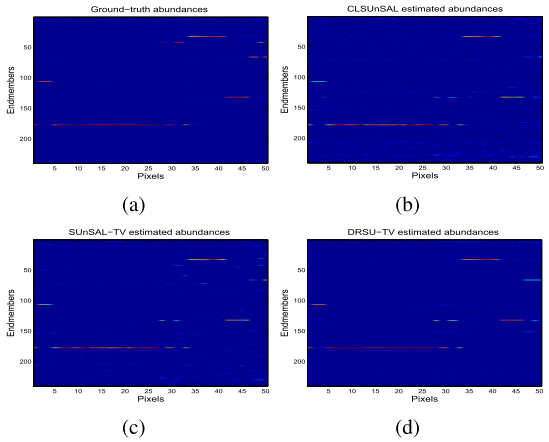

Fig. 4. Ground-truth and estimated abundances obtained for each endmember material in the spectral library for 50 pixels in DC2 when SNR = 20 dB.

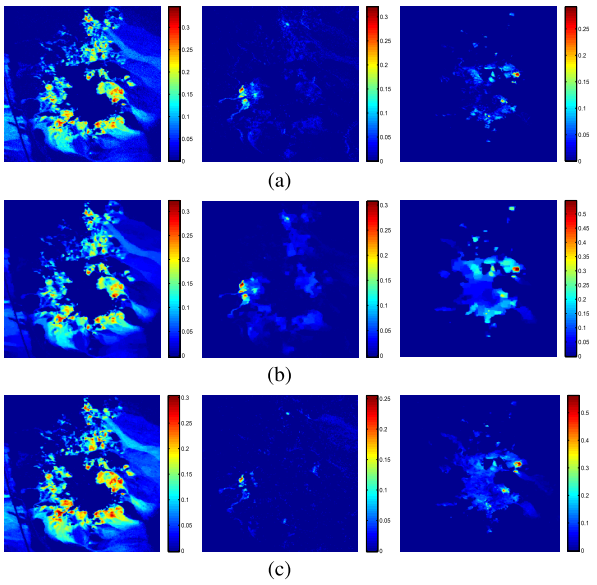

Fig. 5. Fractional abundance maps estimated for the AVIRIS Cuprite subscene with the USGS library. (Left to right) Alunite, Buddingtonite, and Chalcedony. (a) CLSUnSAL. (b) SUnSAL-TV. (c) DRSU-TV.

of fractional abundances simultaneously. The same conclusion can also be confirmed by the observation of Figs. 3 and 4, for which there are less abundance lines of false spectral signatures in the abundance matrix obtained by DRSU-TV than by CLSUnSAL and SUnSAL-TV.

B. Real Data Experiments

The real hyperspectral image used in the experiments is a subset of 250 × 191 pixels and 188 bands from the publicly available Airborne Visible/Infrared Imaging Spectrometer (AVIRIS) Cuprite data collected in 1997. The Cuprite site is well understood mineralogically, and it has several exposed minerals of interest. The standard spectral library for these data is the USGS library containing 498 pure endmember signatures. Essential calibration was undertaken in order to mitigate the mismatch between the hyperspectral image and the signatures in library [7]. The estimated results of CLSUnSAL, SUnSAL-TV, and DRSU-TV are shown in Fig. 5. As evidenced in Fig. 5, three algorithms have shown the good unmixing results. Compared with CLSUnSAL and SUnSAL-TV, our proposed DRSU-TV yields the better abundance maps with high spatial consistency of minerals of interest. The estimated abundances by SUnSAL-TV may exhibit an oversmooth visual effect.

IV. Conclusion

In this letter, we have developed the DRSU-TV algorithm to address the hyperspectral unmixing problem, for which the newly introduced double weights improve the sparsity of the endmembers in spectral library and abundance fraction of every endmember, while the TV-based regularization enforces the spatial smoothness of abundance map. The underlying optimization problem is solved by the ADMM. The experimental results show that the DRSU-TV algorithm substantially improves the unmixing performance with regard to the state-of-the-art techniques. Future work will focus on how to choose the parameters adaptively for the DRSU-TV algorithm.

References

[1] J. B. Adams, M. O. Smith, and P. E. Johnson, "Spectral mixture modeling: A new analysis of rock and soil types at the Viking Lander 1 site," *J. Geophys.*, vol. 91, no. B8, pp. 8098–8112, 1986.

[2] A. Plaza, Q. Du, J. M. Bioucas-Dias, X. Jia, and F. A. Kruse, "Foreword to the special issue on spectral unmixing of remotely sensed data," *IEEE Trans. Geosci. Remote Sens.*, vol. 49, no. 11, pp. 4103–4110, Nov. 2011.

[3] N. Keshava and J. F. Mustard, "Spectral unmixing," *IEEE Signal Process. Mag.*, vol. 19, no. 1, pp. 44–57, Jan. 2002.

[4] D. C. Heinz and C.-I. Chang, "Fully constrained least squares linear spectral mixture analysis method for material quantification in hyperspectral imagery," *IEEE Trans. Geosci. Remote Sens.*, vol. 39, no. 3, pp. 529–545, Mar. 2001.

[5] J. M. Bioucas-Dias *et al.*, "Hyperspectral unmixing overview: Geometrical, statistical, and sparse regression-based approaches," *IEEE J. Sel. Topics Appl. Earth Observ. Remote Sens.*, vol. 5, no. 2, pp. 354–379, Apr. 2012.

[6] J. M. Bioucas-Dias and M. A. T. Figueiredo, "Alternating direction algorithms for constrained sparse regression: Application to hyperspectral unmixing," in *Proc. WHISPERS*, Reykjavik, Iceland, Jun. 2010, pp. 1–4.

[7] M.-D. Iordache, J. M. Bioucas-Dias, and A. Plaza, "Sparse unmixing of hyperspectral data," *IEEE Trans. Geosci. Remote Sens.*, vol. 49, no. 6, pp. 2014–2039, Jun. 2011.

[8] M.-D. Iordache, J. M. Bioucas-Dias, and A. Plaza, "Total variation spatial regularization for sparse hyperspectral unmixing," *IEEE Trans. Geosci. Remote Sens.*, vol. 50, no. 11, pp. 4484–4502, Nov. 2012.

[9] M.-D. Iordache, J. M. Bioucas-Dias, and A. Plaza, "Collaborative sparse regression for hyperspectral unmixing," *IEEE Trans. Geosci. Remote Sens.*, vol. 52, no. 1, pp. 341–354, Jan. 2014.

[10] F. Chen and Y. Zhang, "Sparse hyperspectral unmixing based on constrained lp-l_2 optimization," *IEEE Geosci. Remote Sens. Lett.*, vol. 10, no. 5, pp. 1142–1146, Jan. 2013.

[11] J. Sigurdsson, M. O. Ulfarsson, and J. R. Sveinsson, "Hyperspectral unmixing with l_q regularization," *IEEE Trans. Geosci. Remote Sens.*, vol. 52, no. 11, pp. 6793–6806, Nov. 2014.

[12] E. J. Candès, M. B. Wakin, and S. P. Boyd, "Enhancing sparsity by reweighted ℓ_1 minimization," *J. Fourier Anal. Appl.*, vol. 14, no. 5, pp. 877–905, 2008.

[13] M. V. Afonso, J. M. Bioucas-Dias, and M. A. T. Figueiredo, "An augmented Lagrangian approach to the constrained optimization formulation of imaging inverse problems," *IEEE Trans. Image Process.*, vol. 20, no. 3, pp. 681–695, Mar. 2011.

[14] Y. G. Peng, J. L. Suo, Q. H. Dai, and W. L. Xu, "Reweighted low-rank matrix recovery and its application in image restoration," *IEEE Trans. Cybern.*, vol. 44, no. 12, pp. 2418–2430, Dec. 2014.

[15] P. L. Combettes and V. R. Wajs, "Signal recovery by proximal forward-backward splitting," *SIAM J. Multiscale Model. Simul.*, vol. 4, no. 4, pp. 1168–1200, Jan. 2005.

[16] B. Kozintsev, "Computations with Gaussian random fields," Ph.D. dissertation, Dept. Math., Univ. Maryland, College Park, MD, USA, 1999.